Indian Journal of Pure & Applied Physics
Vol. 62, October 2024, pp. 918-924
DOI: 10.56042/ijpap.v62i10.8849

2-Methoxy Ethanol-Driven Solvent Engineering of $Cs_3Bi_2I_9$ Perovskite Films and its Impact on Lead Free Perovskite Solar Cell Devices

Anil K Sharma[a], Ambreesh Kumar[a], Jitendra Yadav[a],Upendra Chauhan[a], Savita[a,b], Maikesh Mathur[c], Hari P Bhasker[c], Punit K Dhawan[b], Shiv P Patel[d] & Dhirendra K Chaudhary[a*]

[a]Centre for Renewable Energy, Prof. Rajendra Singh (Rajju Bhaiya) Institute of Physical Sciences for Study and Research, V. B. S. Purvanchal University, Jaunpur 222 003, India

[b]Department of Physics, Prof. Rajendra Singh (Rajju Bhaiya) Institute of Physical Sciences for Study and Research, V. B. S. Purvanchal University, Jaunpur 222 003, India

[c]Department of Physics, Chowdhary Mahadeo Prasad Degree College, University of Allahabad, Allahabad 211 002, India

[d]Department of Pure & Applied Physics, Guru Ghasidas Vishwavidyalaya (A Central University), Bilaspur 495 009, India

Received 16 February 2024; accepted 1 August 2024

The development of compact perovskite thin films is essential for fabrication of high-performance solar cell devices. Solvent engineering stands out as a promising method to achieve such films, providing a straightforward approach with significant control over the film formation process. In this study, we employed a solvent engineering approach to attain compact and uniform growth in $Cs_3Bi_2I_9$ films. We incorporated 2-methoxy ethanol (2-ME) as an additive in N, N-Dimethylformamide (DMF) solvent. The resulting perovskite films exhibited enhanced crystallinity and absorbance compared to films prepared with DMF alone, particularly when using a DMF:2-ME mixing ratio of 4:1. Moreover, we successfully fabricated lead-free, flexible perovskite solar cell devices using a solution processing technique. The photovoltaic performance of estimated and efficiency of devices prepared with 4:1 ratio of DMF:2-ME exhibited efficiency of ~1.56%.

Keywords: Solvent engineering; Semi-transparent Solar cells; Lead-free perovskite solar cells; Flexible solar cells

1 Introduction

Perovskite solar cell technology has demonstrated its remarkable potential, achieving an efficiency of ~ 25.5%, which is comparable to commercially available solar cell devices. However, the majority of high-efficiency devices are fabricated using lead (Pb)-based perovskites[1-4]. It is important to mention here that the presence of lead gives rise to a few crucial challenges related to the environment due to its toxicity and water solubility[5], raising concerns about its environmental impact and potential harm to human health[6-8]. As a result, the development of lead-free perovskite materials and their solar cell devices has become a challenging area of research.

Bismuth (Bi)-based perovskite appears to be one of the very promising lead-free alternative materials. Bismuth (Bi^{3+}) shares a stable electronic configuration ($6s^2$ $6p^0$) similar to lead (Pb^{2+}), allowing it to effectively mask charge defects within the material. In this configuration, the empty p-orbital of bismuth serves as the conduction band, while the filled 6s orbital, combined with the 5p orbital of iodide (I), forms the valence band[9]. Such an electronic band structure provides a potential avenue for the development of efficient and environmentally friendly perovskite materials for photovoltaic applications.

In recent years, several studies have reported the fabrication and characterization of lead-free bismuth-based perovskite[9-17]. Shin *et al.* utilized a solvent engineering approach to fabricate perovskite thin films with different chemical compositions, including methylammonium bismuth iodide (MBI), forma-midinium bismuth iodide (FBI), and cesium bismuth iodide (CBI), for perovskite solar cells[9]. They employed dimethyl sulfoxide (DMSO) and 4-tert Butylpyridine (tBP) as anti-solvents in dimethyl-formamide (DMF) and achieved promising results with MBI-based solar cells demonstrating an open-circuit voltage (Voc) of approximately 0.85 V and a power conversion efficiency (PCE) of ~0.7%[10]. Fan *et al.* reported the fabrication of $(FA)_3Bi_2I_9$ perovskite films using DMF and DMSO solvents, observing the formation of more compact films when DMSO was utilized[11]. Furthermore,

*Corresponding author:
(E-mail: phydhiru005@gmail.com; dhiren@vbspu.ac.in)

Johansson et al. optimized the ratios of CsI/BiI_3 in the perovskite composition and investigated different blending[12]. Hu et al. studied band engineering in one-dimensional antimony/bismuth-based organic-inorganic hybrids by suitably modifying the metal and halogen ratios according to Vegard's law[13].

In addition to these, there are several other studies that have explored the growth of lead-free perovskite single crystals. *Wang et al.* reported the growth of $Cs_3Bi_2I_9$ single crystal thin films using a space-limited solvent evaporation crystallization method[14]. Their findings suggested a significant increase in high mobility and a trap density of approximately 5.7×10^{12} cm^{-1}. *Islam et al.* investigated solvent engineering and anti-solvent treatment techniques for $CsBi_3I_{10}$ perovskite, leading to extended absorption up to 700 nm and a reduced bandgap of approximately 1.75 eV[15]. Hou *et al.* explored the impact of solvents on bismuth-based perovskites and fabricated a compact $Cs_2AgBiBr_6$ film with a large grain size, resulting in an efficiency of approximately 0.73% and ~40% enhancement in power conversion efficiency[16]. In recent years, a lot of work has been carried out using 2-methoxyethanol (2-ME) as a processing solvent for the growth of compact perovskite films[17-19]. 2-ME exhibits higher volatility, enabling the rapid drying of $Cs_3Bi_2I_9$ perovskite films compared to conventional solvents[17].

Extensive research has been dedicated to advancing lead-free perovskite solar cell devices, yet exploration of semi-transparent lead-free solar cell technology remains scarce. To realize cost-effective and non-toxic building-integrated solar cell solutions, this particular area of perovskite solar cell development requires further exploration.

In this study, we employed a solvent engineering technique to grow a dense perovskite film utilizing 2-ME with DMF solvents. The used method accelerates the drying process of the perovskite thin film, yielding a film with larger grain size. By meticulously optimizing the blending ratio, we effectively manufactured semi-transparent flexible perovskite solar cells, achieving power conversion efficiency (PCE) of 1.56%. Our findings underscore the potential of utilizing 2-ME for solvent engineering in lead free Perovskite solar cell devices, highlighting its application in semi-transparent lead-free solar cell technology.

2 Experimental Details

2.1 Materials

All the chemicals such as Cesium Iodide (CsI), Bismuth Iodide (BiI_3), N, N-Dimethylformamide (DMF), 2- Methoxyethanol, Zinc Acetate Hexa Hydrate, PEDOT: PSS, Ethanol were procured from Sigma Aldrich and Ti-nanoxide (T/SP, particle size 20 nm) were purchased from Solaronix and used without any further purification.

2.2 Perovskite Precursor Solution

For the preparation of perovskite precursor solution, Cesium iodide (CsI) and Bismuth iodide (BiI_3) in molar ratio 3:2 was mixed in dimethyleformamide (DMF) and different ratio of 2-ME. Then resulting solution was stirred at 60 °C overnight for getting uniform solution.

2.3 ZnO Precursor Solution

A solution of $Zn(CH_3COO)_2.2H_2O$ in 2-methoxy ethanol were prepared in 80gm/ml concentration. Thereafter, solution subjected to stirring at room temperature after getting homogeneous solution. 20µL mono-ethanolamine was drop-wise added under constant stirring which yields a transparent solution. This solution was kept overnight at constant stirring and used after filtering with 0.45 µm PVDF filter.

2.4 Device Fabrication

First of all, the bottom contact was prepared by patterning ITO-coated PET substrates in the desired shape using a chemical etching method. The substrates were masked, and a solution of hydrochloric acid and zinc dust was applied for 60 seconds to etch the ITO layer. Afterward, the substrates underwent thorough washing with a mild soap solution followed by rinsing with deionized (DI) water. The substrate was cleaned using standard cleaning procedure. The substrates were sequentially kept in ultrasonic bath in water, acetone, and isopropyl alcohol for 10 minutes each at a temperature of 40 °C, and then dried with N_2 gas. Further, the substrates were tried under UV-ozone lamp for 10 minutes to remove any residual solvents. Since flexible ITO-coated PET substrates were used, so a polycrystalline ZnO compact layer was employed as compact electron transport layer. For the growth of polycrystalline ZnO thin films, a 200 µl ZnO precursor solution was uniformly deposited on the pre-cleaned substrates via spin coating at 3500 RPM for 60 seconds. Subsequently, the coated substrates were annealed at 155 °C for two hours. Then, a mesoporous-TiO_2(mp-TiO_2) solution was deposited onto the ZnO-coated substrates at 2000 RPM for 60 minutes, followed by annealing at 125 °C for 2 hours.

The perovskite precursor solution was then deposited onto the mp-TiO_2-coated substrates at 2500 RPM for 60 seconds, followed by annealing at 90 °C for 80 minutes to promote the formation of the perovskite thin film. Then, the water-free PEDOT:PSS layer on perovskite thin film was deposited using spin coating process at 2000 RPM for 60 seconds, and the substrates were subsequently annealed at 100 °C. In order to define the active area of the device a mechanical scribing method was employed.

2.5 Material and Solar Cell Device Characterization

The UV-Vis absorption spectra of the films were recorded using a Motras (UV Plus) UV-Vis. spectrometer. The crystallographic characterization of the films were analyzed using a Rigaku Smartlab high-resolution X-ray diffractometer with a Cu Kα source. The microscopic imaging and elemental mapping of the films were performed using a Tescan $MAIA_3$ field emission scanning electron microscope (FE-SEM) equipped with an Oxford EDX detector. The device performance was evaluated under calibrated AM 1.5 sunlight with a light intensity of 100 mW cm^{-2}. The light source was calibrated using a National Renewable Energy Laboratory (NREL) standard silicon reference cell. The current density-voltage (J–V) curves were recorded using a Kanopy K-Lyte potentiostat at a scan rate of 0.3 V s^{-1}, without any additional time delay.

3 Results and Discussion

The solar cell devices were fabricated using an all-solution processing approach. Fig. 1(a) depicts the method used for processing the perovskite film on flexible PET substrates. The PET substrates were initially attached to the glass substrates, and then sequentially all other layers were deposited. Subsequently, the PET substrates were detached from the glass substrates for photovoltaic performance measurements.

Thin film fabrication on PET substrates involved the sequential deposition of different layers. Fig. 1(b) displays the simulated crystal structure of the $Cs_3Bi_2I_9$ perovskite film. The schematic arrangement of the conventional architecture semi-transparent perovskite device is shown in Fig. 1(c). Here, the ITO-coated PET substrate serves as the transparent flexible substrate and ZnO/mp-TiO_2 acts as the electron transport layer while $Cs_3Bi_2I_9$ functions as the photoactive layer, and water-free PEDOT: PSS acts as the hole transport and top electrode. Generally, a hole transport layer/buffer layer should be used between the perovskite and PEDOT: PSS but for better transparency we have not used any addition layer. A photograph of the devices is shown in Fig. 1(d).

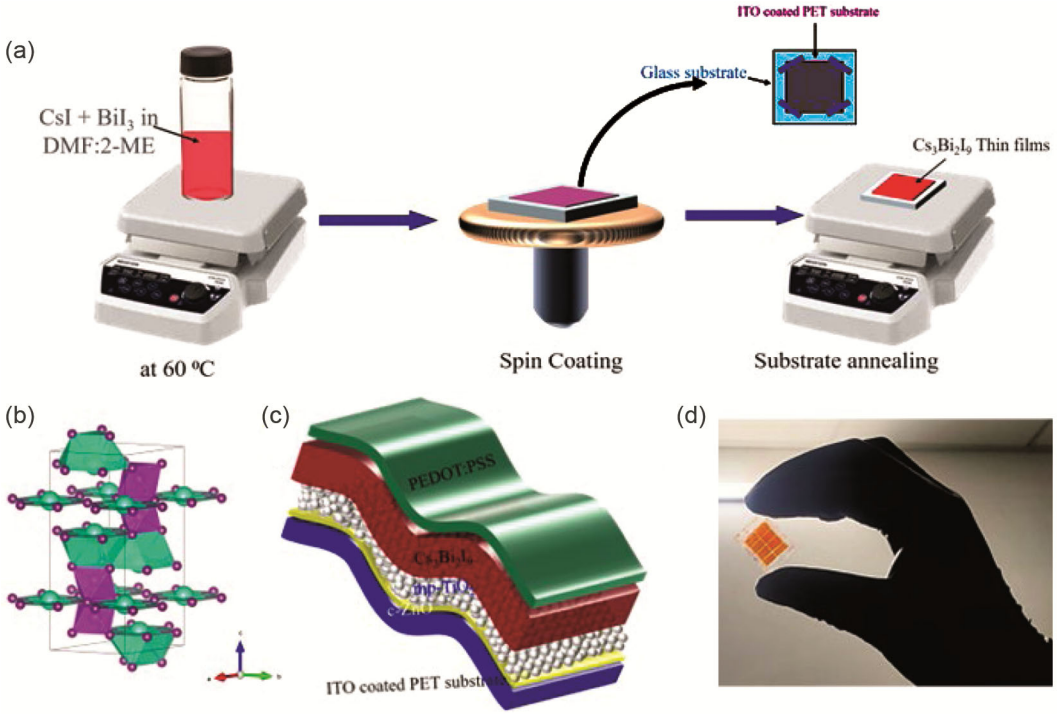

Fig. 1 — (a) Schematic diagram of film processing conditions; (b) Crystal structure of $Cs_3Bi_2I_9$; (c) Schematic diagram of normal architecture semi-transparent flexible solar cell and (d) Photograph of as fabricated solar cell device

The XRD pattern of the as-deposited and 2-ME modified $Cs_3Bi_2I_9$ films is shown in Fig. 2(a). The diffraction peaks observed at positions 12.78°, 16.77°, 25.24°, 26.51°, 27.62°, 37.21°, 42.66°, 51.72°, 61.5°, and 65.55° are assigned to the planes of the hexagonal crystal structure of $Cs_3Bi_2I_9$ (JCPDS Card No. 00-023-0847), corresponding to (101), (004), (006), (114), (203), (302), (0 0 10), (0 0 12), (408), and (2 0 14) crystallographic planes, respectively. No additional peaks corresponding to CsI and BiI_3 were observed in the XRD pattern, indicating that the entire surface is covered with crystalline $Cs_3Bi_2I_9$ exclusively.

A significant enhancement in the peak position in 2-ME modified $Cs_3Bi_2I_9$ films has been observed. A noticeable increase in the intensity of the characteristic peaks was observed compared to the as-grown samples. This enhancement in peak intensity suggests the formation of larger grain sizes in the modified films. The Debye-Scherrer formula was used to estimate the crystallite size of the $Cs_3Bi_2I_9$ films[20]. The estimated value of crystallite size in case of as deposited $Cs_3Bi_2I_9$ films 43±8 nm. Moreover, crystallite size in 2ME treated $Cs_3Bi_2I_9$ films is estimated to be 52±4 nm. This enhancement in crystallite attribute due to accelerated crystal growth. The significant enhancement in peak intensity and the increase in crystallite size indicate improved structural properties in the 2-ME modified $Cs_3Bi_2I_9$ films.

The UV-Vis absorbance spectra and Tauc's plot of the as-deposited and 2-ME modified $Cs_3Bi_2I_9$ films are depicted in Fig. 2(b & c) respectively. The UV-Vis absorption spectra exhibit distinct absorption edges at approximately 595 nm for the as-deposited $Cs_3Bi_2I_9$ films and 622 nm for the 2-ME modified $Cs_3Bi_2I_9$ films. These absorption edges correspond to changes in the band gap of the films. The shift in the absorption edge towards longer wavelengths in the 2-ME modified films indicates a reduced band gap as compared to the as-deposited films. DMF possess vapour pressure ~0.49 kPa at 25 °C and a high boiling point (152-154 °C). Whereas, 2-ME exhibits relatively high vapor pressure ~0.83 kPa at 20 °C with low boiling point (124-125 °C), which accelerates crystal growth and results dense perovskite films with larger grain sizes[17]. These findings are consistent with previous reports and provide additional evidence for the influence of 2-ME modification on the optical properties of $Cs_3Bi_2I_9$ films[17]. The larger grain size increases the distance of light propagation due to backscattering of incident light from the comparatively rough surface, contributes to enhancement in absorbance spectra[20].

Figure 3 illustrates the field emission scanning electron micrographs of the as-deposited and 2-ME modified $Cs_3Bi_2I_9$ films. Fig. 3(a & b) present the topographic and cross-sectional micrographs, respectively for the perovskite films prepared using DMF solvent alone. In the case of the DMF-only solvent, the perovskite films exhibit a fleck-like structure having a wide range of grain sizes (300 nm - 1 μm) with random orientations. The cross-sectional SEM image confirms the growth of $Cs_3Bi_2I_9$ grains with random orientations.

In contrast, the $Cs_3Bi_2I_9$ films prepared using a blend of DMF and 2-ME in a 4:1 ratio exhibits a highly compact and smooth morphology with significantly larger grain sizes (~5 μm). The addition of 2-ME, which has higher volatility compared to DMF, accelerates the crystallization process, resulting in the formation of smoother $Cs_3Bi_2I_9$ perovskite films with larger grain sizes. Furthermore, Fig. 3(e-g) presents the energy-dispersive X-ray (EDX) elemental mapping of Cs, Bi, and I across the cross-sectional area

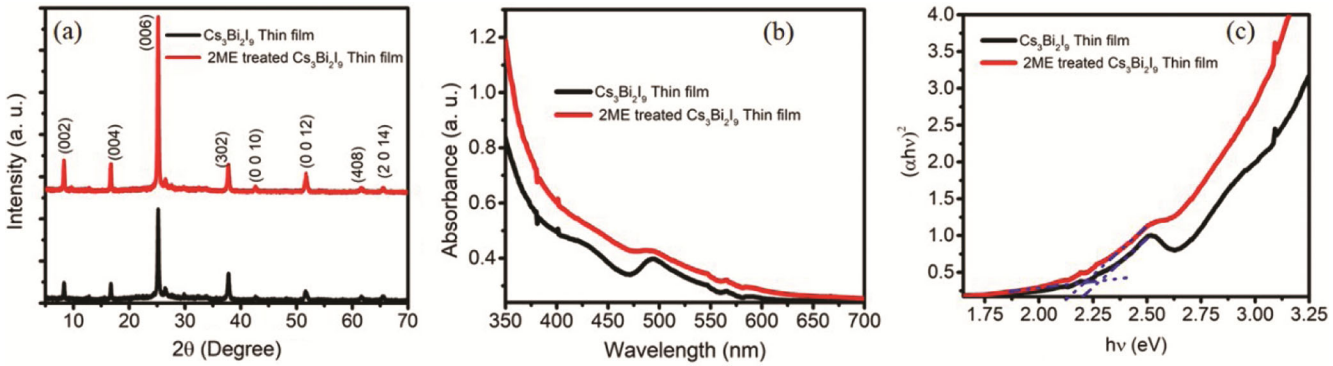

Fig. 2 — (a) XRD diffractogram (b) UV-Vis. absorbance spectra and (c) Tauc plot of$Cs_3Bi_2I_9$perovskite films grown in DMF and DMF:2-ME solvent blended in 4:1 ratio

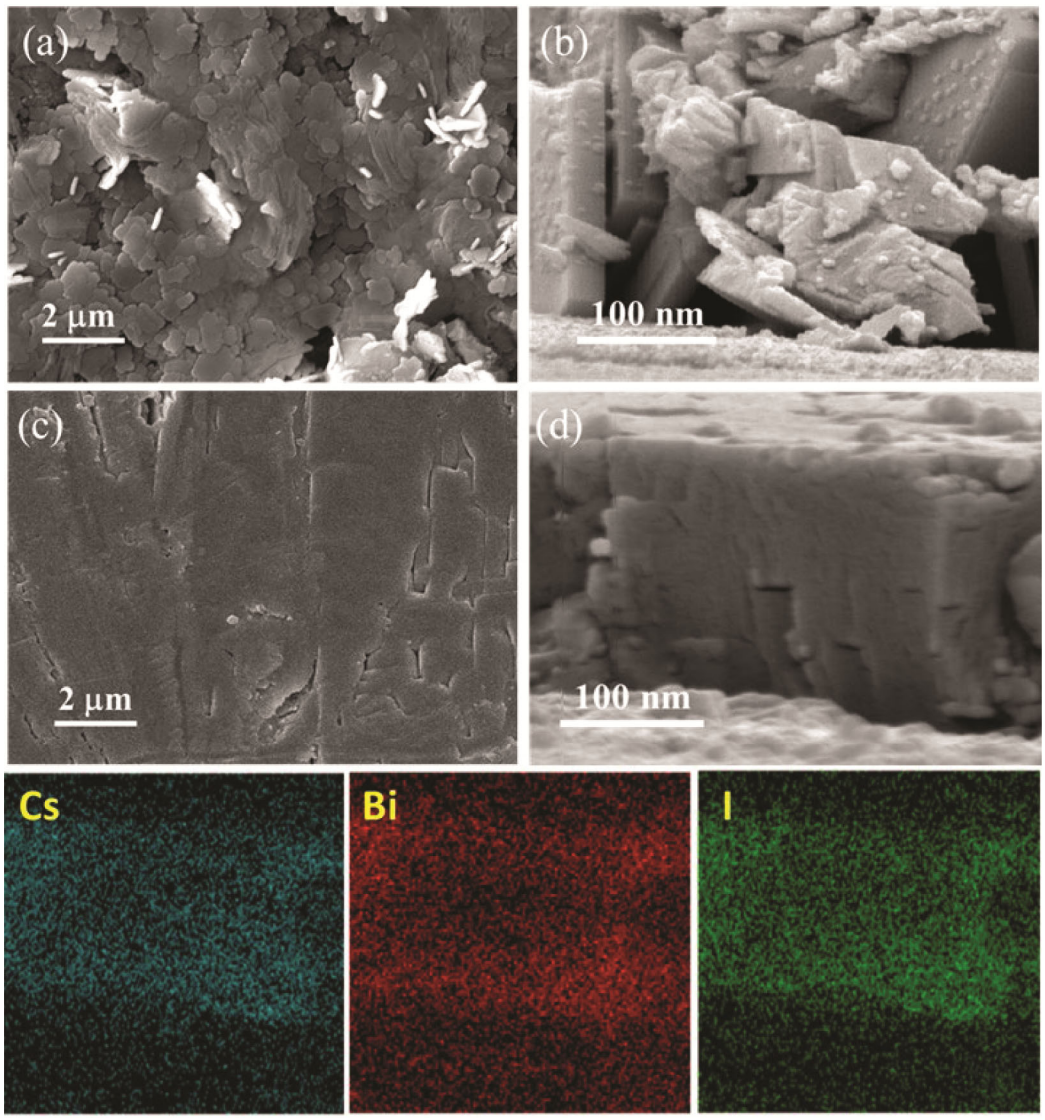

Fig. 3 — Field emission scanning electron micrograph of (a) $Cs_3Bi_2I_9$ perovskite films and (b) cross section of films grown in DMF; (c) $Cs_3Bi_2I_9$ perovskite films and (d) cross section of films grown inDMF:2-ME solvent blended in 4:1 ratio and (e-g) elemental mapping of films grown in DMF:2-ME solvent blended in 4:1 ratio

of the films grown using the DMF:2-ME solvent blend in a 4:1 ratio. The elemental mapping demonstrates the uniform distribution of these elements throughout the film. Additionally, it can be observed that the perovskite solution properly infiltrates the mp-TiO_2 film, indicating good interfacial contact between the layers.

Figure 4(a) displays the dark *J-V* characteristics of the devices while Fig. 4(b) shows the semi-log plot of the dark characteristics. The slope of the trap field region was estimated from the log-log plot of dark characteristics and found to be 4.73 and 7.87 for devices fabricated using perovskite films grown in DMF and DMF:2-ME solvent blended in a 4:1 ratio, respectively. These results suggest that the suppression of trap levels occurs in devices fabricated using perovskite films grown in DMF:2-ME. This suppression may be attributed to the formation of a compact and larger grain size which reduces the trap levels. The larger grain size perovskite offers a lower level of granular boundaries, thereby reducing trap levels. The *J-V* characteristics of the best-performing devices under illumination are shown in Fig. 4(c) and the photovoltaic performance of the devices is shown in Table 1.

The devices fabricated using $Cs_3Bi_2I_9$ films grown in DMF:2-ME exhibit a power conversion efficiency (η) of 1.56% with significant increments in Jsc, Voc, and FF, respectively. The enhancement in efficiency

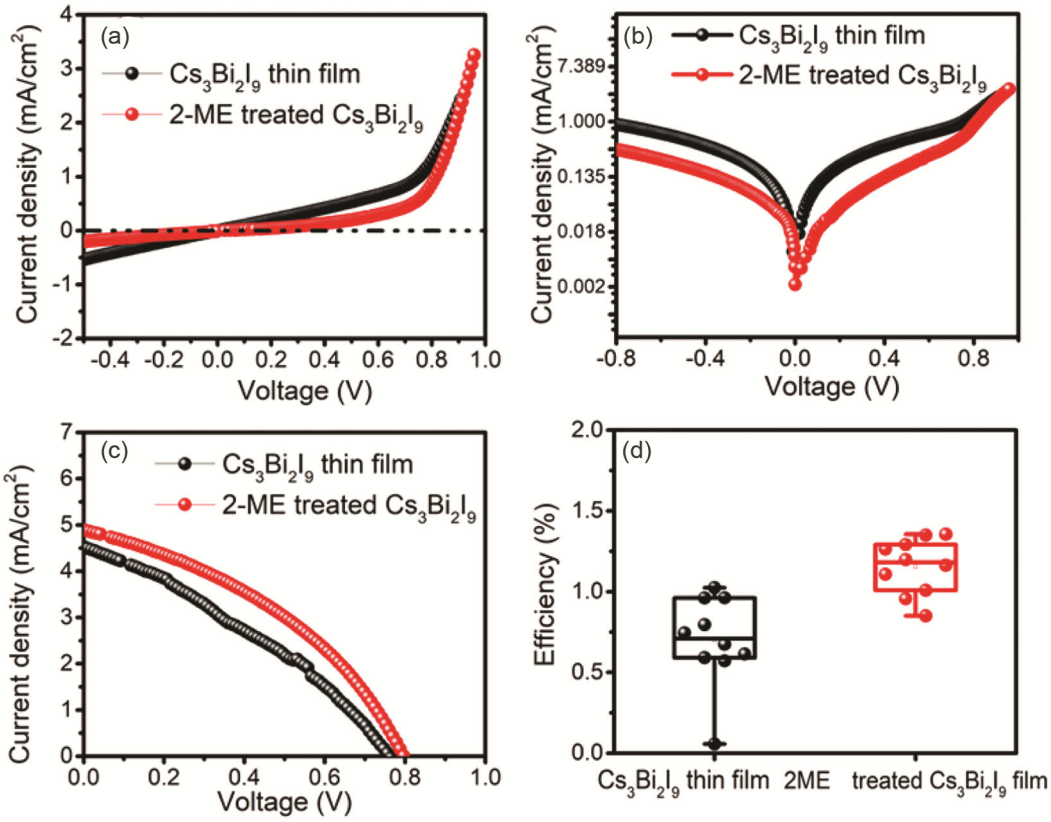

Fig. 4 — (a) Dark J-V characteristics (b) semi-log plot of dark J-V characteristics (c) J-V characteristics of best performing devices under 100 mW/cm^2 illumination conditions and (d) box plot of efficiency of devices fabricated using perovskite films grown in DMF and DMF:2-ME solvent blended in 4:1 ratio in 4 different batches

Table 1 — Photovoltaic performance parameters of solar cell devices under AM 1.5 illumination conditions.

S. No.	$Cs_3Bi_2I_9$ based Flexible solar cells with	J_{sc}(mAcm^{-2})	V_{oc} (Volt)	FF	PCE (%)
1	$Cs_3Bi_2I_9$ films grown in DMF	4.26	0.75	0.32	1.02
2	$Cs_3Bi_2I_9$ films in DMF:2-ME (4:1)	4.90	0.79	0.40	1.56

can be attributed to the improvement in Jsc, Voc, and FF. $Cs_3Bi_2I_9$ films grown in DMF:2-ME exhibit enhanced absorption spectra along with a red shift (Fig. 2(b)). The enhancement in Jsc may be attributed to the improved absorption spectra of $Cs_3Bi_2I_9$ films grown in DMF:2-ME, while the enhancement in Voc can be attributed to the change in bandgap and suppression of trap levels. The FF in devices fabricated using $Cs_3Bi_2I_9$ films grown in DMF:2-ME is also enhanced, which may be attributed to the formation of a larger grain size. The larger and compact grain structure of the perovskite facilitates smooth charge carrier conduction, leading to an improvement in FF.

Fig. 4(d) depicts the box plot of the efficiency of devices fabricated using perovskite films grown in DMF and DMF:2-ME solvent blended in a 4:1 ratio in four different batches. Each batch of fabrication shows the same trend of improvement in device efficiency.

4 Conclusion

In summary, the structural and photovoltaic study of semi-transparent $Cs_3Bi_2I_9$-based flexible perovskite solar cells is presented. Our study suggests that their performance can be enhanced through a solvent engineering method. By the incorporation 2-ME solvent as an additive, the power conversion efficiency of the solar cells was improved to ~1.53%. The addition of 2-ME in the fabrication process played a crucial role in accelerating the rate of crystallization of the thin films, and results the formation of perovskite films with a smooth and compact morphology. These structural improvements are key factors to the enhanced photovoltaic performance of these devices. Overall, the results

highlighted the significance of solvent engineering and the specific role of 2-ME for manipulating the crystallization process of $Cs_3Bi_2I_9$ perovskite films. The achieved improvement in film morphology, grain size, and crystallinity contributes to the observed enhancement in power conversion efficiency of the devices. These findings provide valuable insights for the further advancements for the development of efficient and lead free perovskite solar cell on flexible substrates.

Acknowledgments

Authors acknowledge the financial support from the Council of Science and Technology, Uttar Pradesh under research &development project (Ref. No.: CST/D-2287 dated 02.03.2021). DKC acknowledge Department of Higher Education, Govt. of Uttar Pradesh for support under "Centre of Excellence" grant (9/2022/447/70-4-2022-04(17)/2021 dated 15/03/2022) and University Grant Commission (UGC), New Delhi for the support under Start-up grant (No. F-30-573/2021(BSR) dated 15/06/2022). HP Backnowledge UGC, New Delhi for the support under Start-up grant F.30-461/2019 (BSR) dated 21.05.2019 and central advanced facility for material characterization (CAFMC), Prof. Rajendra Singh (Rajju Bhaiya) Institute of Physical Sciences for characterization of the films.

Conflict of Interest

Authors declare there is no conflict of interest.

References

1 Dharmadasa I M, Rahaq Y & Alam A E, *J Mater Sci: Mater Electron*, 30 (2019) 12851.
2 Zhang Z, Sun Q, Lu Y, Lu F, Mu X, Wei S-H & Sui M, *Nature Commun*, 13 (2022) 3397.
3 Ma S, Yuan G, Zhang Y, Yang N, Li Y & Chen Q, *Energy Environ Sci*, 15 (2022) 13.
4 Guo Z, Jena A K, Kim G M & Miyasaka T, *Energy Environ Sci*, 15 (2022) 3171.
5 Collin M S, Venkatraman S K, Vijayakumar N, Kanimozhi V, S Arbaaz M, Stacey R G S, Anusha J, Choudhary R, Lvov V, Tovar G I, Senatov F, Koppala S & Swamiappan S, *J Hazard Mater Adv*, 7 (2022) 100094.
6 Qiu X, Cao B, Yuan S, Chen X, Qiu Z, Jiang Y, Ye Q, Wang H, Zeng H, Liu J & Kanatzidis M G, *Sol Energy Mater Sol Cells*, 159 (2017) 227.
7 Miyasaka T, Kulkarni A, Kim G M, Öz S & Jena A K, *Adv Energy Mater*, 10 (2020) 1902500.
8 Igbari F, Wang R, Wang Z-K, Ma X-J, Wang Q, Wang K-L, Zhang Y, Liao L-S & Yang Y, *Nano Lett*, 19 (2019) 2066.
9 Park B-W, Philippe B, Zhang X, Rensmo H, Boschloo G & Johansson E M J, *Adv Mater*, 27 (2015) 6806.
10 Shin S S, Baena J P C, Kurchin R C, Polizzotti A, Yoo J J, Wieghold S, Bawendi M G & Buonassisi T, *Chem Mater*, 30 (2018) 336.
11 Lan C, Liang G, Zhao S, Lan H, Peng H, Zhang D, Sun H, Luo J & Fan P, *Sol Energy*, 177 (2019) 501.
12 Johansson M B, Philippe B, Banerjee A, Phuyal D, Mukherjee S, Chakraborty S, Cameau M, Zhu H, Ahuja R, Boschloo G, Rensmo H & Johansson E M J, *Inorg Chem*, 58 (2019) 12040.
13 Hu Y-Q, Hui H-Y, Lin W-Q, Wen H-Q, Yang D-S, Feng G-D, *Inorg Chem*, 58 (2019) 16346.
14 Li W-G, Wang X-D, Liao J-F, Jiang Y & Kuang D-B, *Adv Funct Mater*, 30 (2020) 1909701.
15 Mariyappan P, Chowdhury T H, Subashchandran S, Bedja I, Ghaithan H M & Islam A, *Sustain Energy Fuels*, 4 (2020) 5042.
16 Hou P, Yang W, Wan N, Fang Z, Zheng J, Shang M, Fu D, Yang Z & Yang W, *J Mater Chem C*, 9 (2021) 9659.
17 Hendriks K H, Franeker J J van, Bruijnaers B J, Anta J A, Wienk M M & Janssen R A J, *J Mater Chem A*, 5 (2017) 2346.
18 Guo L, Chen Y, Wang G, Xia Y, Luo D, Zhu Z, Wang C, Dong W & Wen S, *ACS Appl Energy Mater*, 4 (2021) 2681.
19 Yoo J W, Jang J, Kim U, Lee Y, Ji S-G, Noh E, Hong S, Choi M & Seok S I, *Joule*, 5 (2021) 2420.
20 Chaudhary D K, Kumar P & Kumar L, *RSC Adv*, 6 (2016) 94731.